JOM Journal of Optical Microsystems

RESEARCH PAPER

Orientation fluctuation in liquid crystal lenses

Yi-Hsin Lin[a,*] **Wei-Cheng Cheng**[a] **Hung-Shan Chen**[a] **Yu-Jen Wang**[a] **and Xiao Liang**[b]

[a]National Yang Ming Chiao Tung University, College of Electrical and Computer Engineering, Department of Photonics, Hsinchu, Taiwan

[b]Tsinghua University, Department of Chemistry, Beijing, China

ABSTRACT. A large-aperture liquid crystal (LC) lens with low driving voltage and reduced haze was demonstrated. The root cause of haze owing to orientation fluctuations was discussed. Theoretical and experimental results confirm that the elastic constant and the electric field help to minimize the haze. The haze was reduced 50% after considering the materials and applied electric field. The improved imaging quality and MTF results of the LC lens were also demonstrated. The driving voltage was reduced from 80 V_{rms} to 18 V_{rms} by removing the typical buffering layer. The applications of such a LC lens are eyeglasses, head-mounted displays, and near eye displays.

Keywords: liquid crystal; liquid crystal lens; tunable focal length

Paper 23009SS received Jun. 1, 2023; revised Sep. 5, 2023; accepted Sep. 7, 2023; published Sep. 20, 2023.

1 Introduction

Liquid crystal (LC) lenses with electrically tunable focal length attract attention due to their potential in ophthalmic applications, three-dimensional displays, portable imaging system and wearable systems based on head-mounted displays (HMDs).[1–8] The optical mechanism of gradient refractive-index (GRIN) LC lenses mainly results from the electrically adjustable distribution of refractive indices for incident extraordinary wave by means of the orientations of LC directors.[1] The LC lenses are generally limited by (a) polarization dependency of LC materials, (b) a "power law" between aperture size and the lens power, and (c) a dilemma between response time and tunable range of lens power. To overcome those limitations, we proposed a LC lens with a multilayered structure, which exhibits polarization independency, large aperture size, and large tunable range of the lens power without sacrificing response time.[9–12] However, poor imaging performance and high driving voltage (~90 V_{rms}) still hinder practical applications. In our previous experiments, we improved the image performance by adjusting the phase profile of the LC lens as a parabolic one (i.e., single vision lens) at different polarizations of incident light.[8] However, the haze is influential in the image quality of the LC lenses.[13,14] The haze in GRIN LC lenses using nematic LC may results from several reasons: (a) light scattering because of poor alignment of LC directors, which leads to small order parameters of LC molecules, (b) rotation of LC directors in azimuthal direction, which leads to induced ordinary wave as incident extraordinary light passing through a GRIN LC lens, and (c) scattering from orientation fluctuations of LC directors. The orientation fluctuation originates from a thermotropic essential of nematic LCs. Many literatures studied methods to reduce light scattering induced by the orientation fluctuations in LC phase retarders, such as enlargement of operating voltages or

*Address all correspondence to Yi-Hsin Lin, yilin@nycu.edu.tw

magnetic fields, reduction of the LC layer thickness, and enhancement of the anchoring energy to confine the LC directors better to bear the perturbation.[15–18] Here, we would like to address how orientation fluctuation affects the images of the LC lenses and try to reduce the effect of orientation fluctuations. To our knowledge, how the orientation fluctuation affects the LC lens has not been investigated yet. In this paper, we proposed a GRIN LC lens with the aperture size of ~10 mm, low driving voltage as well as reduction of haze. The driving voltage is decreased from 80 V_{rms} to 18 V_{rms} by removing the traditional buffering layer as well as finely controlling the high resistive layer (HRL). The imaging quality and MTF are further improved by reducing the haze or said scattering resulting from orientation fluctuations. The main factors to reduce the haze, including the elastic constant, birefringence, and applied voltages, are also studied. We believe this paper can provide a better understanding for the engineers and researchers to develop better GRIN LC lenses. The applications of GRIN LC lenses are eyeglasses, HMDs, and wearable devices.

2 Sample Fabrication

To demonstrate the orientation fluctuations of the LC lens, we adopted the multilayered structure GRIN LC lens with nematic LC materials. Figure 1(a) shows the cross-section of the LC lens. The structure of the LC lens was composed of two glass substrates with thickness of 0.4 mm, one planar layer of indium tin oxide (ITO) as an electrode, one patterned ITO electrode with circular ITO with a diameter of 9.8 mm and a ring gap of 0.2 mm, a buffering layer of the polyimide (referred to as PI and provided by Daxin) with thickness of few microns, a HRL, two alignment layers to align LC molecules, two LC layers, and one polymeric layer (LCP) as a separator of two LC layers. The materials of LC layers we adopted was nematic LC mixture of LN3 (Tsinghua University, $\Delta n = 0.369$ for $\lambda = 589.3$ nm at 20°C), and the thickness of each LC layer was 50 microns. The HRL was made up of PEDOT-PSS (Agfa, S300) mixed with polyvinyl. The thickness and sheet resistance of HRL was <100 nm and 3 MΩ/sq. The function of HRL was to primarily distribute the electric fields to the entire aperture. As depicted in Fig. 1(a), both surfaces of LCP provide capability of alignments to the LC molecules. Moreover, LCP is optically isotropic to the normally incident light because the optical axes in the bulk regions are parallel to z-direction. The fabrication process of LCP is introduced as follows. We filled nematic LC (Merck, MLC 2144, $\Delta n = 0.2493$ for $\lambda = 589.3$ nm at 20°C), reactive mesogen (Merck, RM 257), and photoinitiator (Merck, IRG-184) at 20:79:1 wt. % ratios into the gap between a pair of ITO glass substrates coated with mechanically buffered polyimide (PI) layers. The buffering (or rubbing) directions at two PI layers on ITO glass substrates were anti-parallel. Thereafter, a voltage of 350 V_{rms} at a frequency (f) of 1 kHz was applied to the sample and then the sample was exposed to UV light (~3 mW/cm^2) for 1 h for photo-polymerization. After photo-polymerization, we peeled off the substrates by a thermal releasing process and obtained a film of LCP with thickness of 50 microns. Besides the LC lens in Fig. 1(a), we also

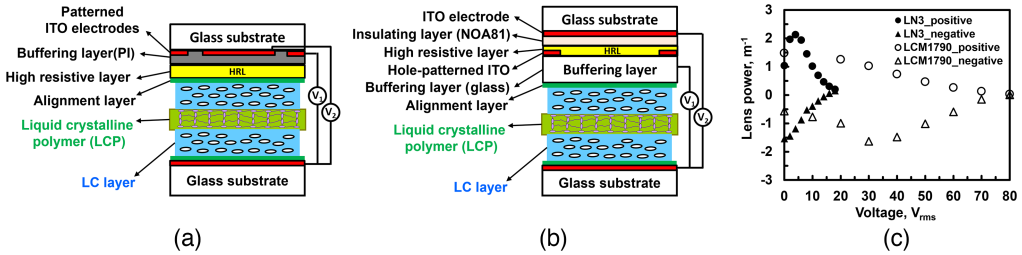

Fig. 1 Illustration of the structures of the LC lens (a) with LN3 and (b) with LCM1790. (c) Lens power of the LC lens as a function of an applied voltage. The lens power is an inverse of the focal length. "Positive" represents the positive lens power by changing $V2$ with fixed ($V1$, frequency) while "negative" represents the negative lens power by changing $V1$ with fixed ($V2$, frequency). The positive lens is operated at $V1 = 18\,V_{rms}$ ($f = 80$ Hz) and $V1 = 80\ V_{rms}$ ($f = 2800$ Hz) for the LC lenses made by LN3 and LCM1790, respectively. The negative lens is operated at $V2 = 18\,V_{rms}$ ($f = 40$ Hz) and $V2 = 80\ V_{rms}$ ($f = 200$ Hz) for the LC lenses made by LN3 and LCM1790, respectively.

fabricated the double-layered structure we proposed in 2014 for comparison.[19] The structure is depicted in Fig. 1(b) whose LC material in the LC layers was LCM1790 (LCMatter Corp., LCM-1790, $\Delta n = 0.4172$ for $\lambda = 589$ nm at 21°C) and the separator was the LCP layer with thickness of 50 microns. Instead of the polarization independent multilayered structure we proposed previously,[9] we adopted a polarization dependent double layered structure where only one eigen-polarization of light could be imaged. The thickness of each LC layer is 50 microns.

To measure the lens power (i.e., an inverse of the focal length) as a function of voltages, a Shack–Hartmann wavefront sensor (Thorlab, WFS-150-7AR) and a 4f system were used to measure the phase difference of the wavefront after light propagates in the LC lenses. An unpolarized He–Ne laser ($\lambda = 532$ nm) was adopted. A linear polarizer with transmissive axis parallel to the long axis of LC molecules was used after the unpolarized He–Ne laser, so the light enters to the LC lens is linearly polarized light (extraordinary wave). The Zernike coefficients were obtained after converting phase difference of wavefront and then the lens power of the LC lens was further calculated by Zernike polynomial fittings.[20] The measured lens power as a function of applied voltage pairs (V_1, V_2) on the LC lens is shown in Fig. 1(c). The hollow and solid legends represent the lens power of LC lenses made of LCM1790 and LN3, respectively. To operate the LN3 sample as a positive lens, we maintained the applied voltage of $V_1 = 18\,V_{rms}$ ($f = 80$ Hz) while changing V_2 ($V_2 < 18\,V_{rms}$). Similarly, the applied voltage of $V_2 = 18\,V_{rms}$ ($f = 40$ Hz) is fixed while changing V_1 ($V_1 < 18\,V_{rms}$) to operate the LC lens as a negative lens. For the LCM-1790 sample, we changed the applied voltage of V_2 ($f = 2800$ Hz) while maintaining V_1 of $80\,V_{rms}$ to function as a positive lens. Similarly, the LC lens functions as a negative lens when we changed the applied voltage of V_1 ($f = 200$ Hz) at $V_2 = 80\,V_{rms}$. The reason why we changed both the frequency and voltage is because the frequency-dependent impedance of HRL. From Fig. 1(b), the lens power of the LC lens of LN3 is capable of being switched from -1.54 D (Diopter or m^{-1}) to $+2.13$ D. The total tunable range is 3.67 D. Besides, the lens power of the LC lens of LCM1790 is capable of being switched from -1.64 D (Diopter or m^{-1}) to 1.48 D. The total tunable range is 3.12 D. The tunable ranges of both LC lenses are similar, but the driving voltage is reduced from $80\,V_{rms}$ to below $18\,V_{rms}$, around 4X reduction. Dielectric anisotropy, the difference between the relative permittivity (or dielectric constant) in the long molecular axis and in the short molecular axis, for LN3 and LCM 1790 are 6 and 18.8, respectively. Larger dielectric anisotropy represents larger induced dipole moment, which leads to easier to be reoriented by applied electric fields. In theory, LC with larger dielectric anisotropy and small elastic constant indicate lower threshold electric field. As a result, the driving voltage in LN3 sample should be higher since the K_{11} is larger and dielectric anisotropy is smaller compared to LCM 1790 sample. However, LN3 sample displays lower driving voltage. This is because the buffering layer of the LC lens of LN3 is replaced by the polyimide with a few microns of thickness to reduce the voltage across the HRL. This explains why the driving voltage is reduced dramatically in LN3 sample compared to LCM 1790 sample.

3 Experimental Results and Discussions

The image is also important to a lens design though the lens power could be measured. However, we found that a fluctuation of the wavefront during the measurement. Such a fluctuation causes some scattering and then it results in haze of image. Thus, we prepared different samples to observe the light scattering of the LC materials. We prepared two cells composed of two ITO glass substrates coated with rubbed polyimide layers (or so-called homogeneous cells. No hole-patterned electrodes). The one cell with cell gap of 41.88 microns is filled with LCM-1790 and the other one with cell gap 43.89 microns is filled with LN3. The unpolarized laser diode ($\lambda = 532$ nm) was impinged onto the samples, where a white screen was placed 25 cm behind a sample for observing the scattering phenomenon of the light, as shown in Figs. 2(a)–2(d) (Video 1, MP4, 2.27 MB). Figures 2(a) and 2(b) respectively represent the scattering of the sample of LCM1790 without and with an applied voltage of $1.4\,V_{rms}$. AC frequency was 1 kHz for LCM1790. Similarly, Figs. 2(c) and 2(d) in LN3 sample without and with an applied voltage of $3.4\,V_{rms}$. AC frequency was 1 kHz for LN3. In Figs. 2(a)–2(d), light is scattered more at voltage-on. Moreover, we observed the fluctuation of scattered light for both samples at voltage-on. The fluctuation in LCM 1790 is more server than the one in LN3.

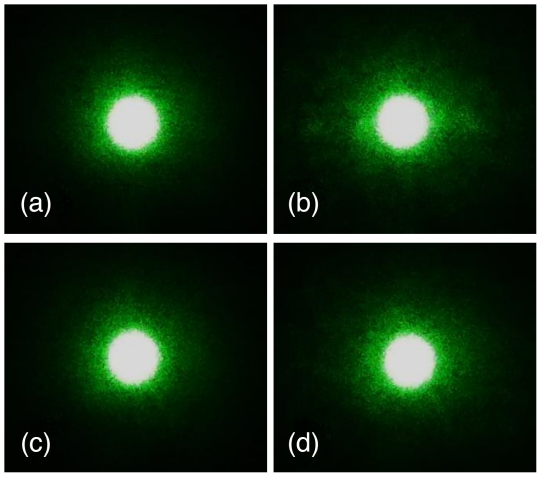

Fig. 2 Observation of light scattering of homogeneous LC cells (Video 1). The sample of LCM1790 at (a) voltage-off and (b) voltage-on (1.4 V_{rms}). The sample of LN3 at (a) voltage-off and (b) voltage-on (3.4 V_{rms}). AC frequency was 1 kHz for LCM1790 and LN3 (Video 1, MP4, 2.27 MB [URL: https://doi.org/10.1117/1.JOM.3.4.041204.s1]).

To quantify the haze, we used a spectral haze meter (SH 7000, NDK) to measure the haze of samples filled with different LCs. Besides two LC materials (LCM-1790 and LN3), we prepared three more homogeneous cells with different LC materials. The related parameters, such as birefringence, splay elastic constant, and cell gaps, were listed in Table 1. The haze in Table 1 is defined as the ratio of the measured transmission of the scattered light to the total transmission of light according to International Organization of Standardization (ISO 14782). The transmission of the scattered light here is defined as a scattered light when the deviation angle of the transmitted light is larger than 2.5 deg.[21] From Table 1, the birefringence and the measured splay elastic constants (K_{11}) of LC materials ranges from 0.22 to 0.42 and 6 to 11 pN, respectively. The cell gaps are 42 μm $\sim$ 44 μm. The splay elastic constant (K_{11}) was calculated in terms of measurement of threshold voltage. As can be seen in Table 1, the measured haze at $\lambda = 550$ nm ranges from 3% to 7%. We also plotted haze as a function of birefringence ($\Delta n = n_e$-n_o) of LC materials in Fig. 3(a). The haze increases with birefringence of LC. We also plotted the haze as a function of splay elastic constant K_{11} in Fig. 3(b). The haze decreases as the elastic constant increases. The haze as a function of $\Delta n^2/K_{11}$ is also plotted in Fig. 3(c). In Fig. 3(c), the haze is almost proportional to ($\Delta n^2/K_{11}$). From Figs. 3(a)–3(c), K_{11} of LC should be large and the LC birefringence should be small in order to reduce the haze. However, the small birefringence of LC leads to a severe reduction of tunable range of the lens power of a LC lens. Furthermore, such a reduction could remove all the lensing effect of the LC lenses, especially when the aperture size is large (>10 mm). Thus, K_{11} of LC has to be large enough to compensate the haze from the birefringence effect to keep the high birefringence of LC. In homogeneous cells, the deformation of nematic LC under electric fields is mainly splay deformation. As a result, we discuss splay elastic constant only. The bend elastic constants for LN3 and LCM 1790 are 25 pN.

Table 1 List of five LC materials and related parameters of LC samples.

LC materials	Δn at $\lambda = 550$ nm	K_{11}, pN	Cell gap (μm)	Haze at $\lambda = 550$ nm
E7	0.22	11.1	42.56	2.78%
MLC 2144	0.25	8.3	42.35	3.11%
MLC 2070	0.26	11.2	42.06	3.62%
LN3	0.37	9	43.89	3.58%
LCM1790	0.42	6	41.88	6.22%

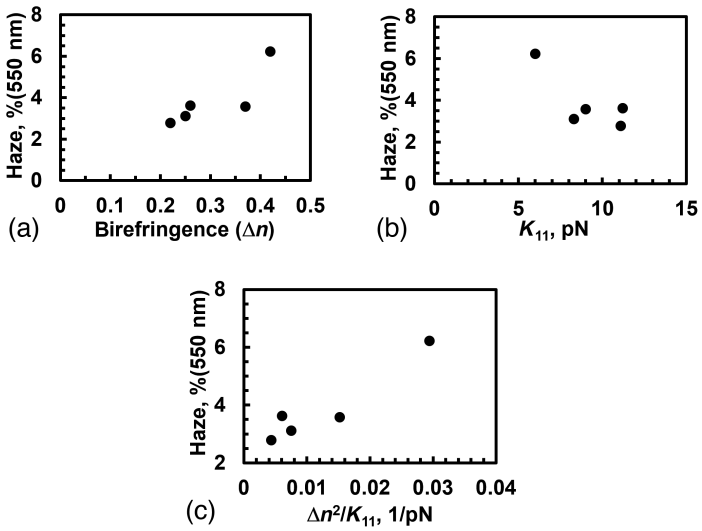

Fig. 3 The haze as a function of (a) birefringence (Δn) and (b) splay elastic constant (K_{11}) and (c) $\Delta n^2/K_{11}$.

To further demonstrate the large K_{11} could reduce the haze of the LC lens from orientation fluctuations, we prepared the LC lenses in Fig. 1 using two LC materials with high birefringence (i.e., LN3 and LCM1790 in Table 1). We measured the haze of the samples at different voltages, as shown in Fig. 4. In Fig. 4, the haze of the LC lens with LCM1790 (solid dotted line) increases with applied voltage as $V < 1.4\,V_{rms}$ and then decreases as $V > 1.4\,V_{rms}$. As to the LC lens with LN3, the haze starts to increase after the voltage exceeds threshold voltage ($2.12\,V_{rms}$). The threshold voltage for the sample of LCM1790 is much smaller than the sample of LN3 because threshold voltage is proportional to $\sqrt{K_{11}/\Delta\varepsilon}$, where $\Delta\varepsilon$ is dielectric anisotropy. The LC directors of LCM1790 are much easier to be oriented or fluctuated by the electric field. As to the reason why the haze goes up near the threshold voltage is because (a) small order parameter of the LC directors near Freedericksz transition results in random orientations of LC directors, and (b) the applied electric field not parallel to the LC directors leads to a magnification of orientation fluctuations of the LC directors. Thereafter, the haze reduces at the higher applied voltage because the reoriented LC directors are more parallel to the electric field and then the orientation fluctuation is reduced. In our previous reports, this also explain that why the image performance is better at the high voltage than at the low voltage.[9] In Fig. 4, the maximum haze of the LCM1790 is around 12% at $1.4\,V_{rms}$, which is two times higher than the maximum haze (~6.74%) of LN3 at $3.4\,V_{rms}$. Based on the elastic continuum theory of nematic LCs, LC needs more energy to perturb the orientations when LC has higher elastic constant. Thus, the LC lens with LC materials of higher K_{11} could reduce haze induced by the orientation fluctuations. This explains why the LC lens using LN3 has smaller haze than the one using LCM1790.

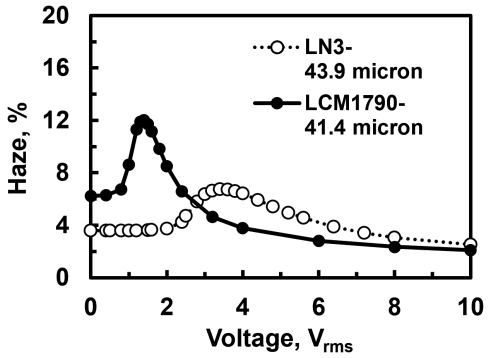

Fig. 4 The haze as a function of applied voltages for two samples: LN3 (hollow dotted line) and LCM1790 (solid dotted line). The cell gaps were 43.9 microns for LN3 sample and 41.4 microns for LCM1790 sample.

The imaging performance of the LC lens is then degraded by orientation fluctuations in terms of noticeable haze. Thermally excited fluctuations of LC directors result in light scattering or haze. According to scattering theory of orientation fluctuation of P. G. de Gennes, the differential scattering cross-section per unit solid angle (σ) of the LCs under the absence of magnetic or electric fields can be roughly estimated as[18]

$$\sigma = \Omega\left(\frac{\varepsilon_a \omega^2}{4\pi c^2}\right)^2 \left(\frac{k_B T}{K q^2}\right), \tag{1}$$

where Ω is the sample volume, ω is the angular frequency, c is the speed of light, k_B is the Boltzmann constant, T is the temperature, K is the elastic constant, and q is the scattering wave vector. ε_a equals to $n_e^2 - n_o^2$. n_e and n_o are extraordinary and ordinary refractive index of LC, respectively. The scattering wave vector q refers to the difference of the wave vectors between incoming and outgoing beams. According to Eq. (1), the scattering is strong when q is small. In the LC lens, the structure of LC layer [Fig. 1(a)] is based on homogeneous alignment. Thereafter, the splay elastic term (K_{11}) dominates the elastic energy of the LC lens. As a result, the K in Eq. (1) is replaced by K_{11}. The larger K_{11} of LC material, the smaller σ. The physical interpretation of smaller scattering could be explained as follows. In the absence of the electric field and surface anchoring force (i.e., thick cell or weak anchoring energy of alignment layers), the free energy in the system consists of elastic energy and thermal energy. To thermally excite fluctuations (or orientation fluctuations) of the LC directors, the thermal energy has to overcome the elastic energy which is confined by K_{11} in the LC layer. We can also regard the force that drives orientation fluctuations as a force of maximum static friction. Besides the elastic constant, the orientation fluctuations could also be suppressed by electric fields, magnetic fields, and anchoring energy of alignment layers. The effect of finite thickness and finite anchoring energy on the light scattering of LC cell was first studied in 1986.[22] The polarization states of the light and scattering wave vector also play important roles in the light scattering.[17] The correlations between angular dependency of the light scattering and elastic constants of the LC materials are also investigated.[16,17] Therefore, the theory could explain the experiment results in Figs. 3 and 4.

To test image performance, the LC lens was attached in front of a camera (Canon 500D EF-S 18 to 55 mm, pixel size: 4.7 μm) to record the image of a resolution chart (USAF 1951) with different spatial frequencies at 25 cm away from the LC lens. The recorded images were further converted to contrast ratio of the recorded image of the resolution chart. The contrast ratio (C) of an image of the resolution chart was defined as

$$C = \frac{I_{\max} - I_{\min}}{I_{\max} + I_{\min}}, \tag{2}$$

where $I_{\max}$ and $I_{\min}$ are the maximum brightness and minimum brightness at a certain spatial frequency, respectively. The contrast ratio as a function of spatial frequency is shown in Fig. 5. The solid circles and hollow triangles respectively represent the contrast ratio for LC lenses made by LN3 and LCM1790, while both LC lens were operated as a negative lens with the lens power approximately -1 D. The operating voltage of the LC lenses made by LN3 and LCM1790 are ($V_1 = 5\,V_{rms}$, $V_2 = 18\,V_{rms}$, 40 Hz) and ($V_1 = 20\,V_{rms}$, $V_2 = 80\,V_{rms}$, 200 Hz), respectively. In Fig. 5, the value of contrast ratio equals 0.2 ($C = 0.2$) at 6.5 lp/mm for the LCM1790 sample, while the $C = 0.2$ was measured at around 24 lp/mm for the LN3 sample. The contrast ratio is improved due to the reduction of the haze or scattering.[23] Two inlets in Fig. 5 are the photos taken at -1 D. From two photos, we can see the image quality of the LN3 sample is much better than the LCM1790 sample. In addition, the impact of aberrations to image quality is still not discussed here under the influence of haze. As mentioned in the Sec. 2, the fluctuation of wavefront occurs during the measurement because of scattering effect. To further improve the imaging quality of the LC lenses, not only the haze but also the wavefront should be carefully modulated. The multiple electrodes can be adopted to control the wavefront.[24–26] To reduce the applied voltage to below $10\,V_{rms}$ while maintaining the low haze performance, LC materials with large dielectric anisotropy at the frequency of ~kHz and with large splay elastic constants can be considered. To minimize the effects of the largely induced haze near the Fréedericksz transition region, few ways can be adopted. The electric field directions inside the LC layer can be designed more parallel to

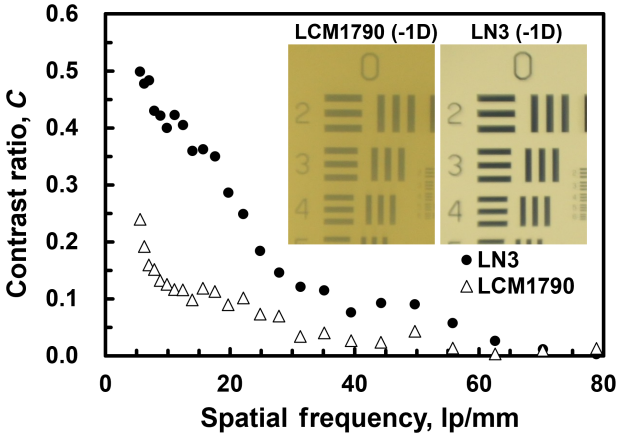

Fig. 5 Image performance and measured contract ratio of the LC lens under an ambient white light (unpolarized light). The solid circles and hollow triangles respectively refer to the improved LC lens (LN3) and old LC lens (LCM-1790) operated at negative lens power of −1 Diopter.

the LC directors, both the elastic constant K_{11} and K_{33} should be properly controlled, or a new LC lens structure should be proposed.

4 Conclusion

We have demonstrated a low driving voltage (<20 V_{rms}) and large aperture size (10 mm) LC lens with reduced haze. The root cause of haze resulting from the orientation fluctuations of LC materials in LC lenses was discussed in this paper. Theoretical and experimental results confirm that the elastic constant and the electric field help to minimize or suppress the haze. The haze can be reduced after considering the materials with large splay elastic constant (K_{11}). The improved imaging quality and contrast ratio results of the LC lens are also demonstrated. On the other hand, the driving voltage is reduced from 80 V_{rms} to 18 V_{rms}. We believe the study paves a way for further applications on imaging systems, such as HMDs and eyeglasses.

Data Availability

Data underlying the results presented in this paper are not publicly available at this time but may be obtained from the authors upon reasonable request.

Acknowledgments

This research was supported by National Sciences and Technology Council (NSTC) in Taiwan (NSTC 112-2112-M-A49-044). The authors are indebted to Google for unrestricted Google Gift.

References

1. D. K. Yang and S. T. Wu, *Fundamentals of Liquid Crystal Devices*, chap. 12, John Wiley & Sons Ltd., Chichester (2006).
2. S. Liu, D. Cheng, and H. Hua, "An optical see-through head mounted display with addressable focal planes," in *Proc. Int. Symp. Mixed and Augmented Reality*, IEEE, pp. 33–41 (2008).
3. Y. H. Lin, M. S. Chen, and H. C. Lin, "An electrically tunable optical zoom system using two composite liquid crystal lenses with a large zoom ratio," *Opt. Express* **19**, 4714–4721 (2011).
4. H. S. Chen and Y. H. Lin, "An endoscopic system adopting a liquid crystal lens with electrically tunable depth-of-field," *Opt. Express* **21**, 18079–18088 (2013).
5. Y. H. Lin and H. S. Chen, "Electrically tunable-focusing and polarizer-free liquid crystal lenses for ophthalmic applications," *Opt. Express* **21**, 9428–9436 (2013).
6. G. Vdovin, M. Loktev, and A. Naumov, "On the possibility of intraocular adaptive optics," *Opt. Express* **11**, 810–817 (2003).
7. Y. J. Wang et al., "Extended depth-of-field 3D endoscopy with synthetic aperture integral imaging using an electrically tunable focal-length liquid-crystal lens," *Opt. Lett.* **40**, 3564–3567 (2015).

8. Y.-J. Wang and Y.-H. Lin, "Liquid crystal technology for vergence-accommodation conflicts in augmented reality and virtual reality systems: a review," *Liq. Cryst. Rev.* **9**(1), 35–64 (2021).
9. H. S. Chen et al., "A polarizer-free liquid crystal lens exploiting an embedded-multilayered structure," *IEEE Photonics Technol. Lett.* **27**, 899–902 (2015).
10. Y.-H. Lin, Y.-J. Wang, and V. Reshetnyak, "Liquid crystal lenses with tunable focal length," *Liq. Cryst. Rev.* **5**(2), 111–143 (2017).
11. Y. J. Wang et al., "Origin of oblique optical axis of electrically tunable focusing lenses arising from initial anisotropic molecular tilts under a symmetric electric field," *AIP Adv.* **10**, 095024 (2020).
12. Y.-J. Wang et al., "Phase modulators with tunability in wavefronts and optical axes originating from anisotropic molecular tilts under symmetric electric field II: experiments," *Opt. Express* **28**, 8985–9001 (2020).
13. H. F. Gleeson, "Light scattering from liquid crystals," in *Handbook of Liquid Crystals*, D. Demus et al., Ed., John Wiley and Sons (2008).
14. P. G. de Gennes, "Long range order and thermal fluctuations in liquid crystals," *Mol. Cryst. Liq. Cryst.* **7**, 325–345 (1969).
15. T. Marusiy et al., "Scattering of light by nematic liquid crystals in cells with a finite energy of the anchoring of the director to the walls," *Sov. Phys. JETP* **64**, 502–507 (1986).
16. A. Valkov and V. Romanov, "Characteristics of propagation and scattering of light in nematic liquid crystals," *JETP* **63**, 737–743 (1986).
17. S. Stallinga et al., "Theory of light scattering by thin nematic liquid crystal films," *Phys. Rev. E* **53**, 6085–6092 (1996).
18. P. G. de Gennes and J. Prost, *The Physics of Liquid Crystals*, Clarendon Press, Oxford (1993).
19. Y. H. Lin, H. S. Chen, C. M. Chang, and Y. J. Wang, "Large aperture and polarizer-free liquid crystal lenses for ophthalmic applications," *Proc. SPIE* **9182**, 91820B (2014).
20. G. M. Dai, *Wavefront Optics for Vision Correction*, SPIE Press (2008).
21. International Organization for Standardization, *ISO 14782-1999: Plastics—Determination of Haze of Transparent Materials*, ISO (1999).
22. T. Ya. Marusii et al., "Scattering of light by nematic liquid crystal in cells with a finite energy of anchoring of the director to the walls," *Zh. Eksp. Teor. Fiz.* **91**, 851–860 (1986).
23. J. W. Goodman, *Introduction to Fourier Optics*, Robert & Company Publishers (2005).
24. T. Galstian et al., "Optical camera with liquid crystal autofocus lens," *Opt. Express* **25**, 29945–29964 (2017).
25. L. Begel and T. Galstian, "Dynamic compensation of gradient index rod lens aberrations by using liquid crystals," *Appl. Opt.* **57**, 7618–7621 (2018).
26. N. Bennis et al., "Aspherical liquid crystal lenses based on a variable transmission electrode," *Opt. Express* **30**, 12237–12247 (2022).

Biographies of the authors are not available.